2016 American Control Conference (ACC)
Boston Marriott Copley Place
July 6-8, 2016. Boston, MA, USA

Aircraft Sensor Fault Detection Using State and Input Estimation

Ahmad Ansari and Dennis S. Bernstein

***Abstract*— This paper presents a method for detecting aircraft sensor faults using state and input estimation. We formulate the kinematics as a nonlinear state space system, which requires no modeling information, and thus is applicable to all aircraft. To illustrate the method, we investigate three fault-detection scenarios, namely, faulty pitot tube, angle-of-attack sensor, and accelerometers. We use the extended Kalman filter for pitot-tube and angle-of-attack sensor fault detection, and retrospective cost input estimation for accelerometer fault detection. For numerical illustration, we use the NASA Generic Transport Model to detect stuck, bias, drift, and deadzone sensor faults.**

I. Introduction

Sensor failure can have catastrophic consequences for systems that operate under feedback control. The tragic crash of Air France flight 447 on June 1, 2009 due to a faulty air-speed sensor is a well-known instance. Techniques for assessing sensor health are thus of intense interest [1–10].

One approach to detecting sensor faults is to use measurements from a set of sensors to estimate a state or input and then compare the estimate to measurements from a suspect sensor that is not used for estimation. In the case where the suspect sensor corresponds to a state of a dynamic system, state estimation techniques, such as the Kalman filter and its nonlinear variants, can be used. In the case where the suspect sensor corresponds to an input of a dynamic system, state estimation techniques that include input estimation can be used. Input estimation techniques are given in [11–17].

The present paper focuses on sensor fault detection for aircraft flight. In this application, two distinct classes of sensors are available. Inertial sensors measure the motion of the vehicle relative to an inertial frame. Relevant sensors include rate gyros, accelerometers, and vertical gyro. Noninertial sensors include position measurements from GPS as well as aerodynamic sensors, such as a pitot tube for measuring forward velocity relative to the air and angle-of-attack (α) and sideslip (β) sensors for measuring the direction of the relative wind in the body frame.

In the present paper we use combinations of inertial and aerodynamic sensors along with state and input estimation techniques to detect sensor faults. This work is motivated by [8,10], which uses rate-gyro, accelerometer, GPS, angle-of-attack, and sideslip measurements to estimate forward velocity relative to the air in order to assess the health of the pitot tube.

Ahmad Ansari, and Dennis S. Bernstein are with the Department of Aerospace Engineering, University of Michigan, Ann Arbor, MI, USA. {ansahmad, dsbaero}@umich.edu

The present paper extends the approach of [8,10] in several ways. First, for pitot-tube fault detection, we apply the extended Kalman filter with augmented bias states in order to deal with biased accelerometer measurements. Unlike [8,10], we do not use GPS to assess the health of the pitot tube. Next, we consider two scenarios that are not considered in [8,10], one of which depends on state estimation and the other on input estimation. In the first scenario, we use the pitot tube, inertial sensors, and β-sensor to assess the health of the α-sensor, whereas, in the second scenario, we use the pitot tube, rate gyros, vertical gyro, α-sensor, and β-sensor to assess the health of the accelerometers. For input estimation in the second scenario, we use a variation of retrospective cost input estimation as described in [18].

II. Problem Formulation

A. Aircraft Kinematics

The Earth frame and aircraft body-fixed frame are denoted by $\mathrm{F_E}$ and $\mathrm{F_{AC}}$, respectively. We assume that $\mathrm{F_E}$ is an inertial frame and the Earth is flat. The origin $\mathrm{O_E}$ of $\mathrm{F_E}$ is any convenient point fixed on the Earth. The axes $\hat{\imath}_{\mathrm{E}}$ and $\hat{\jmath}_{\mathrm{E}}$ are horizontal, while the axis $\hat{k}_{\mathrm{E}}$ points downward. $\mathrm{F_{AC}}$ is defined with $\hat{\imath}_{\mathrm{AC}}$ pointing out the nose of the aircraft, $\hat{\jmath}_{\mathrm{AC}}$ pointing out the right wing, and $\hat{k}_{\mathrm{AC}}$ downward, that is, $\hat{k}_{\mathrm{AC}} = \hat{\imath}_{\mathrm{AC}} \times \hat{\jmath}_{\mathrm{AC}}$. $\mathrm{F_{AC}}$ and $\mathrm{F_E}$ are related by

$$\mathrm{F_{AC}} = \vec{R}_{\mathrm{AC/E}}\, \mathrm{F_E}, \tag{1}$$

where $\vec{R}_{\mathrm{AC/E}}$ is a physical rotation matrix represented by a 3-2-1 Euler rotation sequence, involving two intermediate frames $\mathrm{F_{E'}}$ and $\mathrm{F_{E''}}$. In particular,

$$\vec{R}_{\mathrm{AC/E}} = \vec{R}_{\hat{\imath}_{\mathrm{E''}}}(\Phi)\, \vec{R}_{\hat{\jmath}_{\mathrm{E'}}}(\Theta)\, \vec{R}_{\hat{k}_{\mathrm{E}}}(\Psi), \tag{2}$$

where $\mathrm{F_{E'}} = \vec{R}_{\mathrm{E'/E}}\, \mathrm{F_E}$, $\mathrm{F_{E''}} = \vec{R}_{\mathrm{E''/E'}}\, \mathrm{F_{E'}}$, and $\vec{R}_{\hat{n}}(\kappa)$ is the Rodrigues rotation about the eigenaxis $\hat{n}$ through the eigenangle κ according to the right-hand rule.

At each time instant, let a denote the air particle located at a point that is fixed relative to the aircraft and upstream of the pitot tube. The location of the aircraft center of mass c relative to $\mathrm{O_E}$ at each time instant is given by

$$\vec{r}_{\mathrm{c/O_E}} = \vec{r}_{\mathrm{c/a}} + \vec{r}_{\mathrm{a/O_E}}. \tag{3}$$

Differentiating (3) with respect to $\mathrm{F_E}$ yields

$$\vec{V}_{\mathrm{c}} = \vec{V}_{\mathrm{AC}} + \vec{V}_{\mathrm{a}}, \tag{4}$$

where

$$\vec{V}_{\mathrm{c}} \triangleq \overset{\mathrm{E}\bullet}{\vec{r}}_{\mathrm{c/O_E}}, \quad \vec{V}_{\mathrm{AC}} \triangleq \overset{\mathrm{E}\bullet}{\vec{r}}_{\mathrm{c/a}}, \quad \vec{V}_{\mathrm{a}} \triangleq \overset{\mathrm{E}\bullet}{\vec{r}}_{\mathrm{a/O_E}}. \tag{5}$$

The angular velocity $\vec{\omega}_{\mathrm{AC/E}}$ of $\mathrm{F_{AC}}$ relative to $\mathrm{F_E}$ is related to the rotation matrix $\vec{R}_{\mathrm{AC/E}}$ by Poisson's equation

$$\overset{\mathrm{AC}\bullet}{\vec{R}}_{\mathrm{AC/E}} = \vec{R}_{\mathrm{AC/E}}\,\vec{\omega}^{\times}_{\mathrm{AC/E}}. \tag{6}$$

We resolve $\vec{V}_{\mathrm{AC}}$ and $\vec{\omega}_{\mathrm{AC/E}}$ in $\mathrm{F_{AC}}$ using the notation

$$\begin{bmatrix} U \\ V \\ W \end{bmatrix} \triangleq \vec{V}_{\mathrm{AC}}\Big|_{\mathrm{AC}}, \quad \begin{bmatrix} P \\ Q \\ R \end{bmatrix} \triangleq \vec{\omega}_{\mathrm{AC/E}}\Big|_{\mathrm{AC}}. \tag{7}$$

Resolving the gravity vector $\vec{g}$ in $\mathrm{F_{AC}}$ yields

$$\vec{g}\Big|_{\mathrm{AC}} = \begin{bmatrix} -(\sin\Theta)g \\ (\sin\Phi)(\cos\Theta)g \\ (\cos\Phi)(\cos\Theta)g \end{bmatrix}, \tag{8}$$

where $g = 32.17\,\mathrm{ft/s^2}$. For the Euler rotation sequence 3-2-1 (yaw-pitch-roll), we have

$$\vec{\omega}_{\mathrm{AC/E}}\Big|_{\mathrm{AC}} = \dot{\Phi}\hat{\imath}_{\mathrm{AC}} + \dot{\Theta}\hat{\jmath}_{\mathrm{E}''} + \dot{\Psi}\hat{k}_{\mathrm{E}'}. \tag{9}$$

The acceleration of the aircraft center of mass relative to $\mathrm{O_E}$ is given by

$$\vec{a}_{\mathrm{c/O_E/E}} = \overset{\mathrm{E}\bullet}{\vec{v}}_{\mathrm{c/O_E/E}} = \overset{\mathrm{E}\bullet}{\vec{v}}_{\mathrm{c/a/E}} + \overset{\mathrm{E}\bullet}{\vec{v}}_{\mathrm{a/O_E/E}}. \tag{10}$$

We assume that the ambient wind is spatially uniform and constant with respect to $\mathrm{F_E}$, i.e., $\overset{\mathrm{E}\bullet}{\vec{v}}_{\mathrm{a/O_E/E}} = 0$. Hence

$$\vec{a}_{\mathrm{c/O_E/E}} = \overset{\mathrm{E}\bullet}{\vec{v}}_{\mathrm{c/a/E}} = \overset{\mathrm{E}\bullet}{\vec{V}}_{\mathrm{AC}}. \tag{11}$$

Using the transport theorem with (11) yields

$$\vec{a}_{\mathrm{c/O_E/E}} = \overset{\mathrm{AC}\bullet}{\vec{V}}_{\mathrm{AC}} + \vec{\omega}_{\mathrm{AC/E}} \times \vec{V}_{\mathrm{AC}}. \tag{12}$$

Note that (12) is a kinematic relation that is applicable to all aircraft and is independent of all modeling information.

B. Kinematic Equations

The accelerometer measurement $\vec{a}_{\mathrm{meas}}$ with gravity offset is given by

$$\vec{a}_{\mathrm{meas}} = \vec{a}_{\mathrm{c/O_E/E}} - \vec{g}, \tag{13}$$

where the accelerometers are assumed to be located at the center of mass of the aircraft. Substituting (13) into (12) yields

$$\overset{\mathrm{AC}\bullet}{\vec{V}}_{\mathrm{AC}} = -\vec{\omega}_{\mathrm{AC/E}} \times \vec{V}_{\mathrm{AC}} + \vec{g} + \vec{a}_{\mathrm{meas}}. \tag{14}$$

We resolve $\vec{a}_{\mathrm{meas}}$ in $\mathrm{F_{AC}}$ using the notation

$$\begin{bmatrix} a_x \\ a_y \\ a_z \end{bmatrix} \triangleq \vec{a}_{\mathrm{meas}}\Big|_{\mathrm{AC}}. \tag{15}$$

Resolving (9) in $\mathrm{F_{AC}}$ using (7) yields

$$\begin{bmatrix} P \\ Q \\ R \end{bmatrix} = \begin{bmatrix} 1 & 0 & -\sin\Theta \\ 0 & \cos\Phi & (\cos\Theta)\sin\Phi \\ 0 & -\sin\Phi & (\cos\Theta)\cos\Phi \end{bmatrix} \begin{bmatrix} \dot{\Phi} \\ \dot{\Theta} \\ \dot{\Psi} \end{bmatrix}. \tag{16}$$

The inverse transformation of (16) is given by

$$\begin{bmatrix} \dot{\Phi} \\ \dot{\Theta} \\ \dot{\Psi} \end{bmatrix} = \begin{bmatrix} 1 & (\sin\Phi)\tan\Theta & (\cos\Phi)\tan\Theta \\ 0 & \cos\Phi & -\sin\Phi \\ 0 & (\sin\Phi)\sec\Theta & (\cos\Phi)\sec\Theta \end{bmatrix} \begin{bmatrix} P \\ Q \\ R \end{bmatrix}. \tag{17}$$

Resolving (14) in $\mathrm{F_{AC}}$ using (7), (8), and (15) yields

$$\dot{U} = RV - QW - (\sin\Theta)g + a_x, \tag{18}$$

$$\dot{V} = -RU + PW + (\sin\Phi)(\cos\Theta)g + a_y, \tag{19}$$

$$\dot{W} = QU - PV + (\cos\Phi)(\cos\Theta)g + a_z. \tag{20}$$

Using the components of $\vec{V}_{\mathrm{AC}}$ resolved in $\mathrm{F_{AC}}$, the angle of attack α and sideslip β are given by

$$\alpha = \operatorname{atan2}(W, U), \quad \beta = \operatorname{atan2}(V, \sqrt{U^2 + W^2}). \tag{21}$$

Note that (3)–(21) are exact kinematic equations, and thus are applicable to all rigid aircraft. Note also that (13)–(21) do not include sensor noise.

C. Fault-Detection Scenarios

Table I lists the available on-board sensors for fault detection. A continuous-time state-space model can be formulated using (18)–(21) as

$$\dot{x} = f_{\mathrm{c}}(x, u_{\mathrm{k}}, u_{\mathrm{u}}) + D_1 w, \tag{22}$$

$$y = h(x) + D_2 v, \tag{23}$$

where $x \in \mathbb{R}^{l_x}$ is the unknown state, $u_{\mathrm{k}} \in \mathbb{R}^{l_{u_{\mathrm{k}}}}$ is the known input, $u_{\mathrm{u}} \in \mathbb{R}^{l_{u_{\mathrm{u}}}}$ is the unknown input, $D_1 w \in \mathbb{R}^{l_x}$ is the process noise with covariance $V_1 \triangleq D_1 D_1^{\mathrm{T}} \in \mathbb{R}^{l_x \times l_x}$, $y \in \mathbb{R}^{l_y}$ is the output measurement, and $D_2 v \in \mathbb{R}^{l_y}$ is the measurement noise with covariance $V_2 \triangleq D_2 D_2^{\mathrm{T}} \in \mathbb{R}^{l_y \times l_y}$, and the functions f_{c} and h are known. The process and measurement noise in (22)–(23) arise due to the fact that the measurements are noisy.

Table II defines x, u_{u}, u_{k}, and y for three fault-detection scenarios, in particular, faulty pitot tube, α-sensor, and accelerometers. In each case, the state equations can be written using (18)–(20) and (22) with $l_x = 3$ as

$$\begin{bmatrix} \dot{U} \\ \dot{V} \\ \dot{W} \end{bmatrix} = \begin{bmatrix} RV - QW - (\sin\Theta)g + a_x \\ -RU + PW + (\sin\Phi)(\cos\Theta)g + a_y \\ QU - PV + (\cos\Phi)(\cos\Theta)g + a_z \end{bmatrix} + D_1 w. \tag{24}$$

In the absence of vertical gyro measurements of Φ and Θ, the first two equations in (17) can be integrated to obtain estimates of Φ and Θ. The matrices D_1 and D_2 are determined using Tables I–II and are given as follows;

Scenario 1) Faulty pitot tube:

$$D_1 = \begin{bmatrix} D_{PQR} & D_{\Phi\Theta} & D_{a_x a_y a_z} \end{bmatrix}, \; D_2 = \operatorname{diag}(\sigma_\alpha, \sigma_\beta), \tag{25}$$

where

$$D_{PQR} \triangleq \begin{bmatrix} 0 & -W & V \\ W & 0 & -U \\ -V & U & 0 \end{bmatrix} \begin{bmatrix} \sigma_P & 0 & 0 \\ 0 & \sigma_Q & 0 \\ 0 & 0 & \sigma_R \end{bmatrix},$$

$$D_{\Phi\Theta} \triangleq \begin{bmatrix} 0 & -\cos\Phi \\ -(\sin\Phi)\sin\Theta & (\cos\Phi)\cos\Theta \\ -(\cos\Phi)\sin\Theta & -(\sin\Phi)\cos\Theta \end{bmatrix} \begin{bmatrix} \sigma_\Phi & 0 \\ 0 & \sigma_\Theta \end{bmatrix},$$

$$D_{a_x a_y a_z} \triangleq \begin{bmatrix} \sigma_{a_x} & 0 & 0 \\ 0 & \sigma_{a_y} & 0 \\ 0 & 0 & \sigma_{a_z} \end{bmatrix}.$$

$D_{\Phi\Theta}$ is determined assuming $\sigma_\Phi, \sigma_\Theta$ are small and using the approximations

$$\sin w_\Phi \approx w_\Phi, \; \sin w_\Theta \approx w_\Theta,$$

$$\cos w_\Phi \approx 1, \; \cos w_\Theta \approx 1, w_\Phi w_\Theta = w_\Theta w_\Phi \approx 0,$$

where w_Φ and w_Θ are noise on the measurements or estimates of Φ and Θ, respectively, obtained from (17).

Scenario 2) Faulty α-sensor: D_1 is given by (25) and

$$D_2 = \operatorname{diag}(\sigma_{\mathrm{U}}, \sigma_\beta). \tag{26}$$

Scenario 3) Faulty accelerometer:

$$D_1 = \begin{bmatrix} D_{PQR} & D_{\Phi\Theta} \end{bmatrix}, \; D_2 = \operatorname{diag}(\sigma_{\mathrm{U}}, \sigma_\alpha, \sigma_\beta). \tag{27}$$

TABLE I: On-board sensors for fault detection. The additive noise for each sensor is assumed to be white Gaussian.

Sensors	**Measurements**	**Standard Deviation of Noise**
Pitot Tube	U	σ_U
Rate Gyro	P, Q, R	$\sigma_P, \sigma_Q, \sigma_R$
Vertical Gyro	Θ, Φ	σ_Θ,σ_Φ
Accelerometers	a_x, a_y, a_z	$\sigma_{a_x}, \sigma_{a_y}, \sigma_{a_z}$
α-sensor	α	σ_α
β-sensor	β	σ_β

TABLE II: Scenarios for sensor fault detection

Faulty Sensor	x	y	u_k	u_u
Pitot Tube	U, V, W	α, β	a_x, a_y, a_z P, Q, R Θ, Φ	
α-sensor	U, V, W	U, β	a_x, a_y, a_z P, Q, R Θ, Φ	
Accelero-meter	U, V, W	α, β, U	P, Q, R Θ, Φ	a_x, a_y, a_z

III. State and Input Estimation

In Section II-C, sensor fault detection is formulated as a problem of state and input estimation. We use the extended Kalman filter (EKF) for state estimation and retrospective cost input estimation (RCIE) for input estimation.

The state-space model (22)–(23) can be discretized to first order as

$$x(k+1) = f\left(x(k), u_\mathrm{k}(k), u_\mathrm{u}(k)\right) + \hat{D}_1(k)w(k), \quad (28)$$

$$y(k) = h\left(x(k)\right) + D_2 v(k), \quad (29)$$

where k is the time step, $\bar{D}_1(k) \triangleq T_\mathrm{s} D_1$,

$$f\left(x(k), u_\mathrm{k}(k), u_\mathrm{u}(k)\right) = x(k) + T_\mathrm{s} f_\mathrm{c}\left(x(k), u_\mathrm{k}(k), u_\mathrm{u}(k)\right),$$

and T_s is the sampling time.

A. Extended Kalman Filter (EKF)

EKF consists of two steps. Assuming that $u = u_\mathrm{k}$, that is, the input is fully known, the forecast step is given by

$$x_\mathrm{f}(k) = f\left(x_\mathrm{da}(k-1), u_\mathrm{k}(k-1)\right), \quad (30)$$

$$P_\mathrm{f}(k) = A(k-1)P_\mathrm{da}(k-1)A^\mathrm{T}(k-1) + \bar{V}_1(k-1), \quad (31)$$

where $x_\mathrm{f}(k) \in \mathbb{R}^{l_x}$ is the forecast state, $x_\mathrm{da}(k) \in \mathbb{R}^{l_x}$ is the data assimilation state, $P_\mathrm{f}(k) \in \mathbb{R}^{l_x \times l_x}$ is the forecast error covariance, $P_\mathrm{da}(k) \in \mathbb{R}^{l_x \times l_x}$ is the data assimilation error covariance, $\bar{V}_1 = \bar{D}_1 \bar{D}_1{}^\mathrm{T}$ is the process noise covariance, and $A(k)$ is the Jacobian of f given by

$$A(k) \triangleq \left.\frac{\partial f}{\partial x}\right|_{x_\mathrm{da}(k), u_\mathrm{k}(k)}. \quad (32)$$

The data assimilation step is given by

$$K_\mathrm{da}(k) = P_\mathrm{f}(k)C^\mathrm{T}(k)S_\mathrm{da}^{-1}(k), \quad (33)$$

$$P_\mathrm{da}(k) = P_\mathrm{f}(k) - P_\mathrm{f}(k)C^\mathrm{T}(k)S_\mathrm{da}^{-1}(k)C(k)P_\mathrm{f}(k), \quad (34)$$

$$x_\mathrm{da}(k) = x_\mathrm{f}(k) + K_\mathrm{da}(k)\left[y(k) - h\left(x_\mathrm{f}(k)\right)\right], \quad (35)$$

where $K_\mathrm{da}(k) \in \mathbb{R}^{l_x \times l_y}$ is the state estimator gain, $S_\mathrm{da}(k) \triangleq C(k)P_\mathrm{f}(k)C^\mathrm{T}(k) + V_2(k)$, and $C(k)$ is the Jacobian of h

$$C(k) \triangleq \left.\frac{\partial h}{\partial x}\right|_{x_\mathrm{f}(k)}. \quad (36)$$

B. Retrospective Cost Input Estimation

In the case where the input is partially or fully unknown, (30) does not explicitly account for the unknown input u_u. The effect of $u_\mathrm{u}(k)$ can be included in the process noise $w(k)$ by a suitable choice of $\bar{Q}(k)$. A more effective approach is to estimate $u_\mathrm{u}(k)$ and include it in (30) and (32) with its estimate $\hat{u}_\mathrm{u}(k)$ as

$$x_\mathrm{f}(k) = f\left(x_\mathrm{da}(k-1), u_\mathrm{k}(k-1), \hat{u}_\mathrm{u}(k-1)\right), \quad (37)$$

$$A(k) = \left.\frac{\partial f}{\partial x}\right|_{x_\mathrm{da}(k), u_\mathrm{k}(k), \hat{u}_\mathrm{u}(k)}. \quad (38)$$

In order to estimate $\hat{u}_\mathrm{u}(k)$, we construct an adaptive input estimator that minimizes

$$z(k) \triangleq y(k) - h\left(x_\mathrm{da}(k)\right), \quad (39)$$

where $z(k) \in \mathbb{R}^{l_z}$ is the output error. The estimated input $\hat{u}_\mathrm{u}(k)$ is the output of the *input estimation subsystem* of order n_c given by

$$\hat{u}_\mathrm{u}(k) = \sum_{i=1}^{n_c} M_i^\mathrm{T}(k)\hat{u}_\mathrm{u}^\mathrm{T}(k-i) + \sum_{i=1}^{n_c} N_i^\mathrm{T}(k)z^\mathrm{T}(k-i), \quad (40)$$

where $M_i(k) \in \mathbb{R}^{l_{\hat{u}_\mathrm{u}} \times l_{\hat{u}_\mathrm{u}}}$ and $N_i(k) \in \mathbb{R}^{l_y \times l_{\hat{u}_\mathrm{u}}}$. The subsystem in (40) can be reformulated as

$$\hat{u}_\mathrm{u}(k) = \Phi(k)\theta(k), \quad (41)$$

where $l_\theta \triangleq l_{\hat{u}_\mathrm{u}} n_c (l_{\hat{u}_\mathrm{u}} + l_y)$, and

$$\theta(k) = \mathrm{vec}([M_1^\mathrm{T}(k) \cdots M_{n_c}^\mathrm{T}(k)\ N_1^\mathrm{T}(k) \cdots N_{n_c}^\mathrm{T}(k)]^\mathrm{T}) \in \mathbb{R}^{l_\theta},$$

$$\phi(k) = [\hat{u}_\mathrm{u}^\mathrm{T}(k-1) \cdots \hat{u}_\mathrm{u}^\mathrm{T}(k-n_c)\ y^\mathrm{T}(k-1) \cdots y^\mathrm{T}(k-n_c)]^\mathrm{T},$$

$$\Phi(k) = I_{l_{\hat{u}_\mathrm{u}}} \otimes \phi^\mathrm{T}(k) \in \mathbb{R}^{l_{\hat{u}_\mathrm{u}} \times l_\theta}, \quad (42)$$

where "$\otimes$" denotes the Kronecker product, $\Phi(k)$ is the regressor, and "vec" is the column-stacking operator.

1) Retrospective Performance: Define $G_\mathrm{f}(\mathrm{q}) \triangleq D_\mathrm{f}^{-1}(\mathrm{q})N_\mathrm{f}(\mathrm{q})$, where q is the forward shift operator, $n_\mathrm{f} \geq 1$ is the order of G_f, and

$$N_\mathrm{f}(\mathrm{q}) \triangleq K_1 \mathrm{q}^{n_\mathrm{f}-1} + K_2 \mathrm{q}^{n_\mathrm{f}-2} + \cdots + K_{n_\mathrm{f}}, \quad (43)$$

$$D_\mathrm{f}(\mathrm{q}) \triangleq I_{l_z} \mathrm{q}^{n_\mathrm{f}} + A_1 \mathrm{q}^{n_\mathrm{f}-1} + A_2 \mathrm{q}^{n_\mathrm{f}-2} + \cdots + A_{n_\mathrm{f}}. \quad (44)$$

Furthermore, $K_i \in \mathbb{R}^{l_z \times l_{\hat{u}_\mathrm{u}}}$ for $1 \leq i \leq r$, $A_j \in \mathbb{R}^{l_z \times l_z}$ for $1 \leq j \leq r$, and $\det\left(D_\mathrm{f}(\mathrm{q})\right)$ is asymptotically stable.

Next, for $k \geq 1$, we define the retrospective performance variable

$$\hat{z}(\hat{\theta}, k) \triangleq z(k) + \Phi_\mathrm{f}(k)\hat{\theta} - u_\mathrm{f}(k), \quad (45)$$

where

$$\Phi_\mathrm{f}(k) \triangleq G_\mathrm{f}(\mathrm{q})\Phi(k), \qquad u_\mathrm{f}(k) \triangleq G_\mathrm{f}(\mathrm{q})\hat{u}_\mathrm{u}(k), \quad (46)$$

and $\hat{\theta} \in \mathbb{R}^{l_\theta}$ is determined by optimization below.

2) Markov Parameters: The filter G_f at time step k is based on the input-to-performance transfer matrix $G_{zu_u}(\mathrm{q}, k) = C(k)(\mathrm{q}I - A(k))^{-1}B(k)$, where $A(k)$ is defined by (38), $C(k)$ is defined by (36), and $B(k)$ is the

Jacobian of f with respect to $\hat{u}_{\mathrm{u}}$ evaluated at $\hat{u}_{\mathrm{u}}(k-1)$. For all complex numbers z whose absolute value is greater than the spectral radius of $A(k)$, it follows that

$$G_{zu_{\mathrm{u}}}(\mathrm{z},k) = \sum_{i=0}^{\infty} \frac{H_i(k)}{\mathrm{z}^i}, \tag{47}$$

where, for all, $i \geq 1$, the i^{th} Markov parameter of $G_{zu_u}(\mathrm{z},k)$ is defined by

$$H_i(k) \triangleq C(k)A(k)^{i-1}B(k). \tag{48}$$

At each time step k, G_{f} is chosen to be the finite-impulse-response (FIR) filter

$$G_{\mathrm{f}}(\mathrm{q},k) = \sum_{i=0}^{n_{\mathrm{f}}} \frac{H_i(k)}{\mathrm{q}^i}, \tag{49}$$

obtained by truncating (47).

3) Cumulative Cost and RCIE Update Law: For $k \geq 1$, we define the cumulative cost function

$$J(k,\hat{\theta}) \triangleq \sum_{i=1}^{k} \left(\hat{z}(i)^{\mathrm{T}} R_z \hat{z}(i) + [\Phi(i)\hat{\theta}]^{\mathrm{T}} R_{\hat{u}_{\mathrm{u}}} \Phi(i)\hat{\theta} \right) + [\hat{\theta} - \theta(0)]^{\mathrm{T}} R_\theta [\hat{\theta} - \theta(0)], \tag{50}$$

where R_θ, R_z, and $R_{\hat{u}_{\mathrm{u}}}$ are positive definite. Let $P(0) = R_\theta^{-1}$ and $\theta(0) = \theta_0$. Then, for all $k \geq 1$, the cumulative cost function (50) has the unique global minimizer $\hat{\theta} = \theta(k)$ given by the RLS update

$$\theta(k) = \theta(k-1) - P(k-1)\tilde{\Phi}(k)^{\mathrm{T}}\Gamma(k)^{-1}[\tilde{\Phi}(k)\theta(k-1) + \tilde{z}(k)],$$

where $P(k)$ satisfies

$$P(k) = P(k-1) - P(k-1)\tilde{\Phi}(k)^{\mathrm{T}}\Gamma(k)^{-1}\tilde{\Phi}(k)P(k-1),$$

$$\tilde{\Phi}(k) \triangleq \begin{bmatrix} \Phi_{\mathrm{f}}(k) \\ \Phi(k) \end{bmatrix} \in \mathbb{R}^{(l_z + l_{\hat{u}_{\mathrm{u}}}) \times l_\theta},$$

$$\tilde{R}(k) \triangleq \begin{bmatrix} R_z(k) & 0 \\ 0 & R_{\hat{u}_{\mathrm{u}}}(k) \end{bmatrix} \in \mathbb{R}^{(l_z + l_{\hat{u}_{\mathrm{u}}}) \times (l_z + l_{\hat{u}_{\mathrm{u}}})},$$

$$\tilde{z}(k) \triangleq \begin{bmatrix} z(k) - u_{\mathrm{f}}(k) \\ 0 \end{bmatrix} \in \mathbb{R}^{l_z + l_{\hat{u}_{\mathrm{u}}}},$$

$$\Gamma(k) \triangleq \tilde{R}(k)^{-1} + \tilde{\Phi}(k)P(k-1)\tilde{\Phi}(k)^{\mathrm{T}}.$$

IV. Sensor fault detection

The formulation in sections II–III is applicable to all rigid aircraft. In this paper, we use the NASA Generic Transport Model (GTM) to illustrate sensor fault detection. GTM is a high-fidelity six-degree-of-freedom nonlinear aircraft model with aerodynamic lookup tables [19].

A. Types of sensor faults

We consider the following types of sensor faults:

- *Bias*. The sensor measurement has a constant offset from the true measurement.
- *Drift*. The sensor measurement has a constant-slope deviation from the true measurement.
- *Deadzone*. The sensor reads zero within a specific range.
- *Stuck*. The sensor reading is fixed.

B. Procedure for sensor fault detection

For sensor fault detection using state and input estimation, rich sensor signals are needed. This can be achieved either by exciting the dynamics of the aircraft using its control surfaces or it can arise naturally from the atmosphere, e.g., wind gusts. For this paper, the dynamics of the aircraft are excited using a saturated harmonic elevator input.

For sensor fault detection, we assume the remaining sensors are functional, and we define the residual

$$e(k) \triangleq \sqrt{\sum_{i=k}^{k+k_{\mathrm{w}}} [y(i) - y_{\mathrm{est}}(i)]^2}, \tag{51}$$

where y_{est} is the estimate of y, and k_{w} is the data-window size. We call e as true residual for true value of y, and sensor residual for measured value of y. For each numerical example, $k_{\mathrm{w}} = 1000$ data points, and $x_{\mathrm{da}}(0) = 0.5x(0)$.

V. GTM Examples

We set the sampling time $T_{\mathrm{s}} = 0.01$ s and consider a scenario where GTM is initially trimmed for level flight at an altitude of 8000 ft. We excite the aircraft dynamics using the elevator deflection $\delta e(k) = \mathrm{sat}_2\left[4\,\sin(60kT_{\mathrm{s}} + 45)\right]$ deg, which is a saturated sinusoid with amplitude 4 deg, maximum deflection of ± 2 deg, and a period of 6 s. Unless stated otherwise, the ambient wind is constant with magnitude of 16.88 ft/s.

To emulate sensor noise, we add zero-mean white noise to all of the sensor measurements with standard deviations $\sigma_{a_x} = \sigma_{a_y} = \sigma_{a_z} = 0.01g$, $\sigma_P = \sigma_Q = \sigma_R = 0.01$ rad/s, $\sigma_\Phi = \sigma_\Theta = 0.01$ rad, $\sigma_\alpha = \sigma_\beta = 0.01$ rad, and $\sigma_U = 1.0$ ft/s.

To show the fault and noise level, we plot the true measurement and sensor measurement together. We also present the true residual to show the accuracy of the estimates. Note that in practical application, the true measurement and thus the true residual are not available. However, the sensor residual can be used in practice for fault detection.

A. Fault Detection for Pitot-Tube Failure

In the following cases, the pitot tube fails by becoming stuck at the constant value of 160 ft/s, beginning at 100 s.

First we estimate U with noisy input and output measurements. Fig. 1 shows that the true residual decreases to 2 ft/s, indicating that EKF is operating correctly. However, the sensor residual jumps after the sensor fails.

Next, to see the effect of accelerometer bias, we consider the case with accelerometer bias $b_{a_x} = b_{a_y} = b_{a_z} = 0.01g$. Fig. 2 shows that the estimated pitot-tube measurement drifts due to the biased accelerometers. In order to deal with these biases, the dynamics in (22) are augmented as

$$\dot{x} = f_{\mathrm{c}}(x, u_{\mathrm{k}}, u_{\mathrm{u}}) + \hat{b} + D_1 w, \quad \dot{\hat{b}} = 0, \tag{52}$$

where $\hat{b} \in \mathbb{R}^3$ is the estimated bias in the accelerometers. Fig. 3 shows that, with the augmented states, the true residual is less than 2 ft/s, thus indicating no drift in the estimate of U. Consequently, $\hat{b}$ converges to the accelerometer bias.

B. Fault Detection for α-sensor Failure

We now present cases where the α-sensor has either a bias or deadzone beginning at $t = 100$ s. We estimate α using

$$\hat{\alpha} = \mathrm{atan2}(\hat{W}, \hat{U}), \tag{53}$$

where $\hat{W}$ and $\hat{U}$ are the state estimates of (24).

First, we consider the case where the α-sensor has a bias

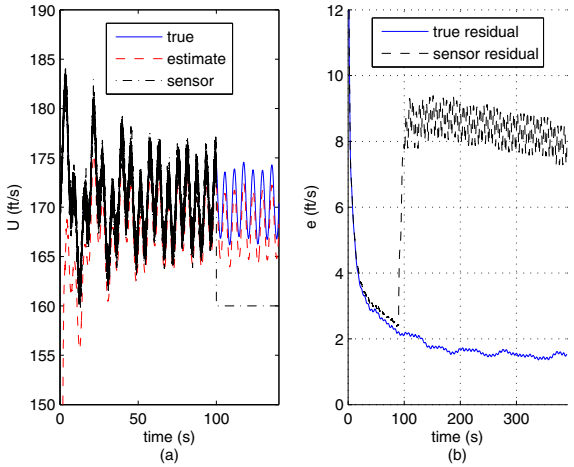

Fig. 1: Stuck pitot tube. (a) At 100 s, the sensor measurement is stuck at 160 ft/s. (b) The sensor residual jumps to a mean value of 8.5 ft/s indicating pitot-tube failure.

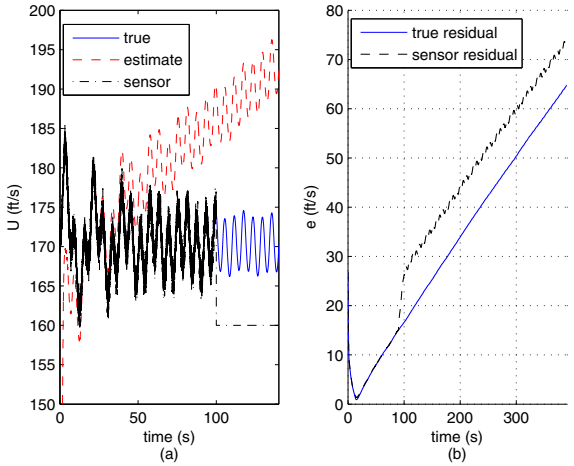

Fig. 2: Estimation of U with biased accelerometers. (a) The estimate of U drifts from the true measurement. Beginning at 100 s, the sensor measurement is stuck at 160 ft/s. (b) The true and sensor residuals are both increasing, and therefore it is not possible to detect the sensor fault. This shortcoming is overcome in Fig. 3.

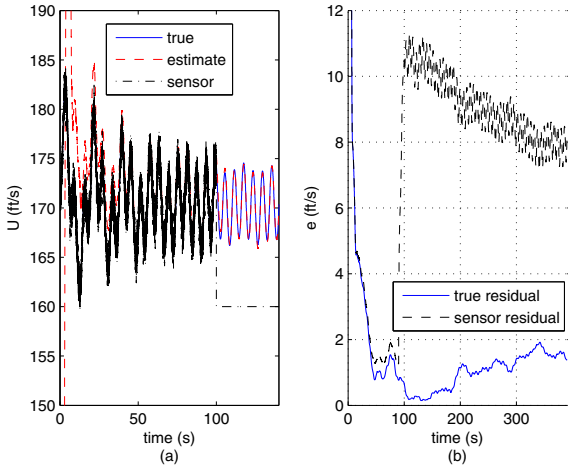

Fig. 3: Estimation of U with augmented bias states. (a) The estimate of U indicates no drift. Beginning at 100 s, the sensor measurement is stuck at 160 ft/s. (b) The true residual is less than 2 ft/s, whereas the sensor residual has an offset due to the stuck fault.

of 4 deg. Fig. 4 shows that the true residual is less than 0.8

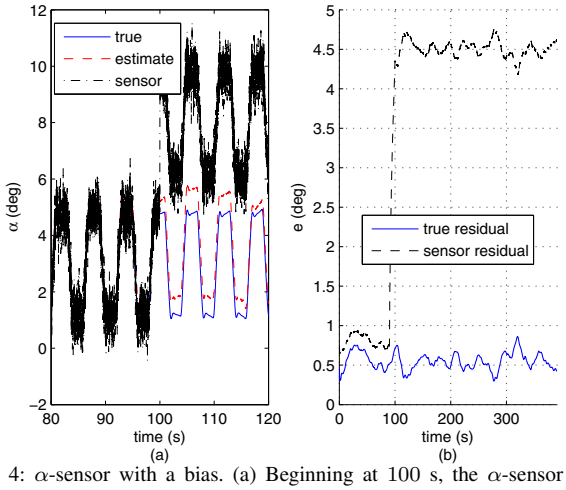

Fig. 4: α-sensor with a bias. (a) Beginning at 100 s, the α-sensor has a bias of 4 deg. (b) The sensor residual indicates an offset due to the bias.

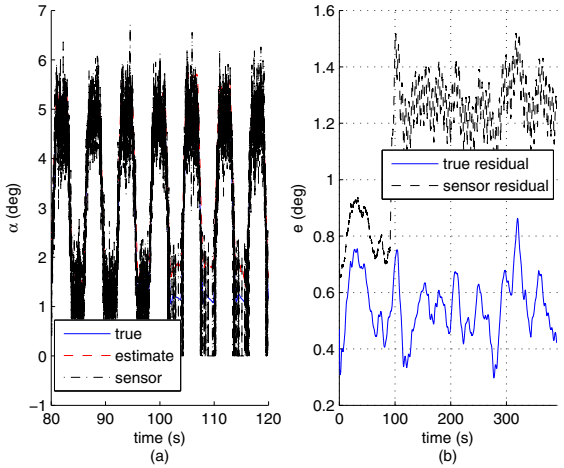

Fig. 5: α-sensor with a deadzone. (a) Beginning at 100 s, the α-sensor reads zero within ± 2 deg. (b) The sensor residual indicates an offset due to the deadzone.

deg, and the sensor residual jumps to 4.5 deg due to the bias.

Next, we consider the deadzone case where the α-sensor reads zero within ± 2 deg. Fig. 5 shows that the sensor residual has an offset due to the deadzone.

C. Fault Detection for Accelerometer Failure

For accelerometer fault detection, we use RCIE to estimate acceleration. To do so, we filter U and augment the states in (24) with an additional filtered state U_{f} as

$$\dot{U}_{\mathrm{f}} = -\omega_{\mathrm{c}}(U_{\mathrm{f}} - U), \tag{54}$$

where $\omega_{\mathrm{c}} > 0$ is the cutoff frequency. We use U_{f} as the output measurement. We choose $\omega_{\mathrm{c}} = 2\pi$ rad/s, $n_{\mathrm{c}} = 6, n_{\mathrm{f}} = 6, R_\theta = 10^{-6} I_{l_\theta}$, and $R_u = 10^{-3}$. Furthermore, we choose $R_z = 1$ and $R_z = 100$ to estimate a_x and a_z, respectively.

We consider cases where the accelerometer has either a bias or drift beginning at 100 s. Fig. 6 shows that RCIE is able to estimate a_x and a_z. Figs. 7a and 8a show cases where a_x and a_z have biases of $0.05g$ and $0.1g$, respectively. Note that the sensor residuals have offsets due to these biases. Figs. 7b and 8b show cases where the measurements of a_x and a_z drift with a slope of 0.001 g/s. Note that the sensor residuals also drift from the respective true residuals.

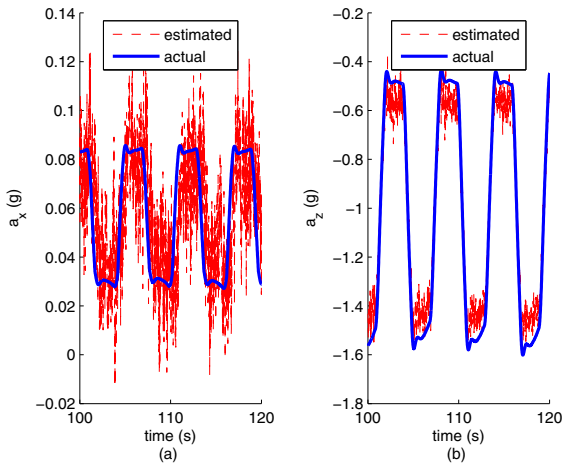

Fig. 6: Acceleration estimation using RCIE. Note that, RCIE is able to estimate a_x and a_z. (a) Estimation of a_x. (b) Estimation of a_z.

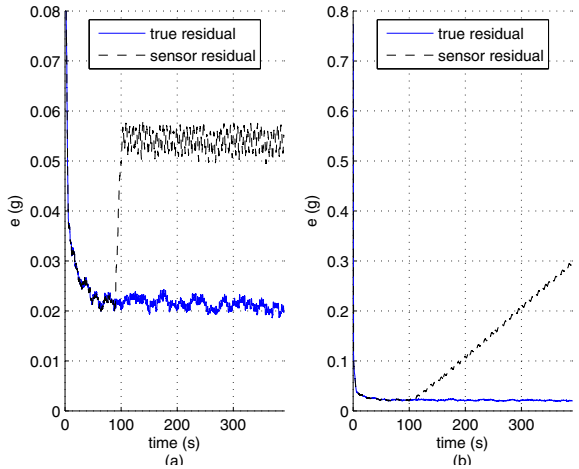

Fig. 7: a_x-sensor. (a) The measurement of a_x is subject to a bias. Note that the sensor residual jumps at 100 s when the bias begins. (b) The measurement of a_x is subject to a drift. Note that the sensor residual begins to increase at 100 s when the drift begins.

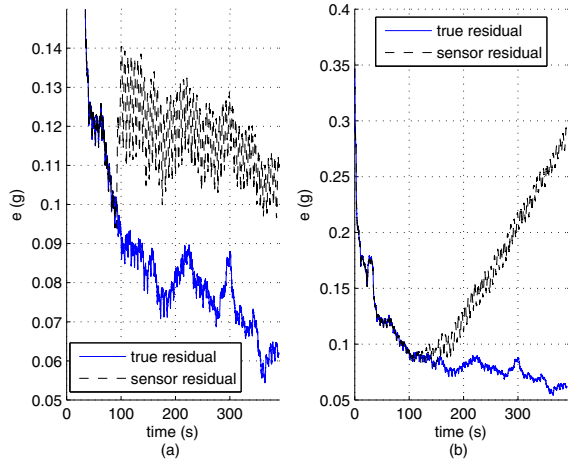

Fig. 8: a_z-sensor. (a) The measurement of a_z is subject to a bias. Note that the sensor residual jumps at 100 s when the bias begins. (b) The measurement of a_z is subject to a drift. Note that the sensor residual begins to increase at 100 s when the drift begins.

VI. Conclusions

In this paper, we presented a method for detecting aircraft sensor faults using state and input estimation. We used the extended Kalman filter (EKF) and retrospective cost input estimation (RCIE) to estimate states and inputs, respectively. For the estimation framework, we used the kinematics to formulate a nonlinear state space system.

Three fault-detection scenarios, in particular, faulty pitot tube, angle-of-attack sensor, and accelerometers were investigated. We used EKF for pitot tube and angle-of-attack sensor fault detection, and RCIE for accelerometer fault detection. In order to illustrate sensor fault detection, we used the NASA Generic Transport Model and presented cases for detecting stuck, bias, drift, and deadzone sensor faults. For all cases, we showed that the sensor residual can be used to detect sensor faults.

VII. Acknowledgment

This research was supported in part by the Office of Naval Research under grant N00014-14-1-0596.

[1] R. Isermann, "Process fault detection based on modeling and estimation methods-a survey," *Automatica*, vol. 20, pp. 387–404, 1984.
[2] A. M. Agogino, S. Srinivas, and K. M. Schneider, "Multiple sensor expert system for diagnostic reasoning, monitoring and control of mechanical systems," *Mech. Sys. Sig. Proc.*, vol. 2, pp. 165–185, 1988.
[3] D. Zhou and P. Frank, "Fault diagnostics and fault tolerant control," *IEEE Trans. Aerosp. Elec. Sys.*, vol. 34, pp. 420–427, 1998.
[4] J. Gertler, *Fault Detection and Diagnosis in Engineering Systems*. CRC press, 1998.
[5] R. Isermann, *Fault-Diagnosis Systems: An Introduction from Fault Detection to Fault Tolerance*. Springer, 2006.
[6] Y. Zhang and J. Jiang, "Bibliographical review on reconfigurable fault-tolerant control systems," *Ann. Rev. Contr.*, vol. 32, pp. 229–252, 2008.
[7] P. Freeman, P. Seiler, and G. J. Balas, "Air data system fault modeling and detection," *Contr. Engr. Pract.*, vol. 21, pp. 1290–1301, 2013.
[8] S. Gururajan, M. Fravolini, M. Rhudy, A. Moschitta, and M. Napolitano, "Evaluation of sensor failure detection, identification and accommodation (SFDIA) performance following common-mode failures of pitot tubes," *SAE Technical Paper*, Sept 2014.
[9] M. L. Fravolini, M. Rhudy, S. Gururajan, S. Cascianelli, and M. Napolitano, "Experimental evaluation of two pitot free analytical redundancy techniques for the estimation of the airspeed of an uav," *SAE Int. Jr. of Aerosp.*, vol. 7, pp. 109–116, 2014.
[10] M. B. Rhudy, M. L. Fravolini, Y. Gu, M. R. Napolitano, S. Gururajan, and H. Chao, "Aircraft model-independent airspeed estimation without pitot tube measurements," *Aerosp. and Elec. Sys., IEEE Transactions on*, vol. 51, pp. 1980–1995, 2015.
[11] M. Corless and J. Tu, "State and input estimation for a class of uncertain systems," *Automatica*, vol. 34, pp. 757–764, 1998.
[12] Y. Xiong and M. Saif, "Unknown disturbance inputs estimation based on a state functional observer design," *Automatica*, vol. 39, pp. 1389–1398, 2003.
[13] T. Floquet and J. P. Barbot, "State and unknown input estimation for linear discrete-time systems," *Automa.*, vol. 42, pp. 1883–1889, 2006.
[14] S. Gillijns and B. De Moor, "Unbiased minimum-variance input and state estimation for linear discrete-time systems," *Automatica*, vol. 43, pp. 111–116, 2007.
[15] H. Palanthandalam-Madapusi and D. S. Bernstein, "A subspace algorithm for simultaneous identification and input reconstruction," *Int. J. Adaptive Contr. Sig. Proc.*, vol. 23, pp. 1053–1069, 2009.
[16] S. Kirtikar, H. Palanthandalam-Madapusi, E. Zattoni, and D. S. Bernstein, "Delay input and initial-state reconstruction for discrete-time linear systems," *Circ. Sys. Sig. Processing*, vol. 30, pp. 233–262, 2011.
[17] H. Fang, R. A. de Callafon, and J. Cortes, "Simultaneous input and state estimation for nonlinear systems with applications to flow field estimation," *Automatica*, vol. 49, pp. 2805–2812, 2013.
[18] A. M. D'Amato and D. S. Bernstein, "Adaptive forward-propagating input reconstruction for nonminimum-phase systems," *Proc. Amer. Conf. Contr.*, pp. 598–603, Montreal, 2012.
[19] T. Jordan, W. Langford, C. Belcastro, J. Foster, G. Shah, G. Howland, and R. Kidd, "Development of a dynamically scaled generic transport model testbed for flight research experiments," *AUVSI Unmanned Unlimited, Arlington, VA*, 2004.